Identification of a KLF5-dependent program and drug development for skeletal muscle atrophy

Lin Liu[a,b], Hiroyuki Koike[a], Takehito Ono[c], Shinichiro Hayashi[d], Fujimi Kudo[e], Atsushi Kaneda[f], Hiroyuki Kagechika[g], Ichiro Manabe[e], Tomoki Nakashima[c], and Yumiko Oishi[a,1]

[a]Department of Biochemistry & Molecular Biology, Nippon Medical School, Tokyo 113-8602, Japan; [b]Department of Cellular and Molecular Medicine, Tokyo Medical and Dental University, Tokyo 113-8510, Japan; [c]Department of Cell Signaling, Graduate School of Medical and Dental Sciences, Tokyo Medical and Dental University, Tokyo 113-8510, Japan; [d]Department of Neuromuscular Research, National Institute of Neuroscience, National Center of Neurology and Psychiatry, Tokyo 187-8551, Japan; [e]Department of Systems Medicine, Chiba University Graduate School of Medicine, Chiba 260-8670, Japan; [f]Department of Molecular Oncology, Chiba University Graduate School of Medicine, Chiba 260-8670, Japan; and [g]Institute of Biomaterials and Bioengineering, Tokyo Medical and Dental University, Tokyo 101-0062, Japan

Edited by Margaret Buckingham, Institut Pasteur, Paris, France, and approved July 20, 2021 (received for review February 15, 2021)

Skeletal muscle atrophy is caused by various conditions, including aging, disuse related to a sedentary lifestyle and lack of physical activity, and cachexia. Our insufficient understanding of the molecular mechanism underlying muscle atrophy limits the targets for the development of effective pharmacologic treatments and preventions. Here, we identified Krüppel-like factor 5 (KLF5), a zinc-finger transcription factor, as a key mediator of the early muscle atrophy program. KLF5 was up-regulated in atrophying myotubes as an early response to dexamethasone or simulated microgravity in vitro. Skeletal muscle–selective deletion of *Klf5* significantly attenuated muscle atrophy induced by mechanical unloading in mice. Transcriptome- and genome-wide chromatin accessibility analyses revealed that KLF5 regulates atrophy-related programs, including metabolic changes and E3-ubiquitin ligase-mediated proteolysis, in coordination with Foxo1. The synthetic retinoic acid receptor agonist Am80, a KLF5 inhibitor, suppressed both dexamethasone- and microgravity-induced muscle atrophy in vitro and oral Am80 ameliorated disuse– and dexamethasone-induced atrophy in mice. Moreover, in three independent sets of transcriptomic data from human skeletal muscle, *KLF5* expression significantly increased with age and the presence of sarcopenia and correlated positively with the expression of the atrophy-related ubiquitin ligase genes *FBXO32* and *TRIM63*. These findings demonstrate that KLF5 is a key transcriptional regulator mediating muscle atrophy and that pharmacological intervention with Am80 is a potentially preventive treatment.

muscle atrophy | KLF | RAR ligand

Skeletal muscle atrophy is a clinical manifestation of the muscle loss due to wasting and catabolism caused by disuse related to a sedentary lifestyle and lack of physical activity as well as to conditions such as cachexia. In particular, sarcopenia, which is characterized by progressive and generalized aging-related loss of skeletal muscle mass and strength, is a growing health and medical burden in aging societies (1). While downstream effectors in the muscle atrophy program, such as the ubiquitin E3 ligases, have been identified, the transcriptional/epigenetic program that governs muscle atrophy remains insufficiently understood. Consequently, the current pharmacologic targets for treating muscle atrophy are very limited (2). Development of improved approaches to treatment will require elucidation of the regulatory mechanisms governing muscle atrophy.

Skeletal muscle is a highly adaptive tissue. It can adapt to physical load through hypertrophy and cope with stress and injury incurred through daily activities. For instance, skeletal muscles are frequently bruised as a result of the mechanical stresses associated with daily living, and even slight skeletal muscle injury can lead to muscle cell death. To maintain muscle mass, skeletal muscle has robust reparative and regenerative mechanisms, including myoblast proliferation and differentiation. Muscle mass is also being constantly regulated by the balance between protein synthesis and degradation. Under conditions leading to prolonged catabolism, such as denervation, cancer, diabetes, fasting, and disuse, the imbalance between protein synthesis and degradation results in muscle atrophy. Ubiquitin-dependent proteolysis is the major pathway leading to muscle fiber breakdown. While this pathway is weakly active in the normal physiological state (3), the cardiac and skeletal muscle–specific E3 ubiquitin ligases, TRIM63 (MuRF1) and FBXO32 (Atrogin-1), are induced and break down damaged myofibrillar proteins in various pathological states (4–6). Mice lacking either *Trim63* or *Fbxo32* showed resistance to muscle atrophy, confirming the particular importance of those genes in the pathogenesis of muscle atrophy (5, 7). Previous studies have identified several transcription factors that regulate *Trim63* and *Fbxo32*, including the Forkhead box protein (Foxo) family of transcription factors, NF-κB, and ZEB-1 (8–10). It is likely, however, that these genes are also regulated by other transcription factors that respond to a variety of mechanical and metabolic stimuli and pathological conditions.

The Krüppel-like factor family of transcription factors (KLFs) are a family of C_2H_2-type zinc-finger transcription factors. KLFs have diverse biological functions during stress responses, embryonic development, and cell proliferation and differentiation (11). Among those functions, KLF2, KLF3, KLF4, KLF5, KLF7, and KLF15 have been shown to play various roles in skeletal muscle biology (12–14). For example, we previously showed that KLF5 has a dual role in skeletal muscle: it controls lipid

Significance

Skeletal muscle atrophy occurs as a result of a variety of conditions including aging, disuse, and cachexia. In this study, we show that the transcription factor KLF5 is transiently up-regulated by metabolic and disuse stimulations and plays a pivotal role in the onset of muscle atrophy in vitro and in vivo. KLF5 physically interacts with Foxo1, and together, they regulate the transcription of *Fbxo32*, a key atrophy-inducing ubiquitin ligase. A synthetic retinoid, Am80, attenuates muscle atrophy in vitro and in vivo. Moreover, publicly available data sets showed that in humans, *KLF5* expression significantly increased with aging and with sarcopenia and correlated positively with expression of the ubiquitin ligase genes *FBXO32* and *TRIM63*.

Author contributions: T.N. and Y.O. designed research; L.L., H. Koike, T.O., S.H., F.K., T.N., and Y.O. performed research; A.K. and H. Kagechika contributed new reagents/analytic tools; L.L., H. Koike, A.K., I.M., and Y.O. analyzed data; and L.L., H. Koike, I.M., and Y.O. wrote the paper.

The authors declare no competing interest.

This article is a PNAS Direct Submission.

[1]To whom correspondence may be addressed. Email: yuooishi@gmail.com.

This article contains supporting information online at https://www.pnas.org/lookup/suppl/doi:10.1073/pnas.2102895118/-/DCSupplemental.

Published August 23, 2021.

metabolism in mature skeletal muscle (15) but also regulates muscle differentiation in myoblasts (16). For the latter, KLF5 is induced in differentiating myoblasts and controls muscle-specific genes in cooperation with MyoD and MEF2. However, the role of KLF5 in the context of muscle atrophy remains unknown.

Several studies published by our group and others have shown that KLF5 function is suppressed by retinoic acid receptor (RAR) agonists, including all-trans retinoic acid and a synthetic RAR agonist, Am80 (17–19). In vascular smooth muscle cells, for instance, KLF5 directly interacts with unliganded RAR to transactivate target genes, while Am80 inhibits KLF5 by disrupting the interaction between KLF5 and RAR. In addition, Am80 decreases the level of *Klf5* expression in some contexts. In the present study, we asked whether KLF5 is involved in muscle atrophy and found that it positively regulates the atrophy program. Moreover, we show that the KLF5 inhibitor Am80 protects mice from unloading-induced muscle atrophy.

Results

KLF5 Is Induced during Muscle Atrophy In Vitro. To begin addressing the possible role of KLF5 in muscle atrophy, we used C2C12 cells, a widely used cultured muscle cell model. The synthetic glucocorticoid dexamethasone (Dex), which induces muscle atrophy in vivo (20), also causes atrophy in differentiated C2C12 myotubes in vitro (21, 22). As expected, when we treated C2C12 myotubes with or without 10 μM Dex for 48 h (Fig. 1*A*), there was a 24% decrease in the average myotube diameter and a reduction in the protein expression of myosin heavy chain (*SI Appendix*, Fig. S1 *A* and *B*). Expression levels of the muscle atrophy–related ubiquitin ligase genes *Fbxo32* and *Trim63* were up-regulated at the messenger RNA (mRNA) and protein levels (*SI Appendix*, Fig. S1 *C* and *D*) (23, 24). Together, these findings confirm that Dex induces atrophy of C2C12 myotubes. In addition, *Klf5* mRNA and KLF5 protein were both up-regulated beginning as early as 4 h after Dex treatment. Moreover, whereas *Klf5* mRNA levels started decrease after 12 h, KLF5 protein expression was maintained for 24 h following Dex treatment (Fig. 1 *B* and *C*). These findings suggest KLF5′s involvement in Dex-induced muscle atrophy in vitro.

Skeletal Muscle–Specific *Klf5* Deficiency Suppresses Unloading-Induced Atrophy In Vivo. The up-regulation of KLF5 in Dex-induced C2C12 myotube atrophy prompted us to investigate the role of KLF5 in skeletal muscle atrophy in vivo. To that end, we generated *Ckm-Cre*;*Klf5*$^{flox/flox}$ conditional knockout (cKO) mice by crossing mice carrying floxed *Klf5* alleles with mice expressing Cre recombinase under the control of the muscle creatine kinase (*Ckm*) promoter. We then assessed the effects of *Klf5* deletion in the gastrocnemius muscle, which is composed largely of fast-twitch fibers, and the soleus muscle, which is composed primarily of slow-twitch fibers. *Klf5* mRNA expression was reduced by ∼80% in cKO gastrocnemius muscle (Fig. 1*D*). Under physiological conditions, cKO mice displayed no obvious phenotypic alterations in the gross appearance. The average gastrocnemius muscle weight in cKO mice tended to be slightly lower than in control mice (e.g., control: 134.48 mg ± 4.83 mg versus cKO: 131.52 mg ± 3.79 mg, $n = 15$ and 13, respectively), though the differences did not reach statistical significance in multiple groups of littermates. The physical activity of the mice and the histology of their gastrocnemius muscles were comparable between the genotypes (*SI Appendix*, Fig. S2 *A–C*), and there were no changes in the fiber type distribution (*SI Appendix*, Fig. S2*D*). Moreover, expression of the muscle contractile gene *Myl2* in gastrocnemius muscle was unaffected by *Klf5* deletion under basal conditions (Fig. 1*I*). It thus appears that although *Klf5* is important for early myocyte differentiation, delayed *Klf5* deletion driven by *Ckm-Cre* (25) appears not to perturb muscle development.

We utilized the tail suspension (TS) model to induce hind-limb atrophy through mechanical unloading and disuse (Fig. 1*E*). We initially analyzed mRNA expression in gastrocnemius muscles during 14 d of TS. As expected, levels of *Klf5*, *Fbxo32*, and *Trim63* expression were increased on day 3 but had started to decrease on day 7. *Klf5* and *Trim63* levels had returned to baseline by day 7, and *Fbxo32* did so by day 14 (Fig. 1*F*). Levels of *Myl2* expression were prominently decreased on day 3 (Fig. 1*F*). These data suggest that expression of genes associated with atrophy is actively altered during the first week in this model. Accordingly, although 1 to 4 wk of TS is often used to induce muscle atrophy (26), we chose a duration of 3 or 7 d based on the gene expression profiles.

Unloading for 3 or 7 d caused reductions in gastrocnemius muscle mass in control mice but not cKO mice (Fig. 1*G* and *SI Appendix*, Fig. S2*E*). The average short diameter was significantly shortened in control mice following unloading for 3 or 7 d but not in the cKO mice (Fig. 1*H*). While the ubiquitin ligases *Fbxo32* and *Trim63* were induced in both control and cKO gastrocnemius, their expression levels in the muscle were significantly lower of cKO than control mice on days 3 and 7 (Fig. 1 *I* and *J*). In addition, expression of *Myl2* was significantly decreased in control mice following unloading for 3 or 7 d, whereas the level of *Myl2* expression was maintained in cKO mice, even on day 7 (Fig. 1*I*). The weight of the soleus muscle was also significantly decreased in control mice but not in cKO mice (*SI Appendix*, Fig. S2 *F* and *G*). *Klf5* mRNA levels were also increased in soleus muscle from control mice after TS (*SI Appendix*, Fig. S2*H*). Collectively, these results demonstrate that muscle-specific *Klf5* deletion attenuates muscle atrophy induced by mechanical unloading.

KLF5 Is Required for Dex-Responsive Gene Expression in Muscle Atrophy. To investigate the mechanisms responsible for KLF5-induced muscle atrophy, we made use of cultured satellite cell (SC)-derived myotubes from cKO mice. Primary SCs were obtained from cKO and control mice, differentiated into myotubes for 2 d in differentiation medium, and then treated with 10 μM Dex for 24 h (Fig. 2*A*). *Klf5* expression was not decreased in undifferentiated SCs derived from cKO mice. *Ckm-Cre* efficiently reduced *Klf5* expression beginning on day 2, presumably due to the delayed induction of *Ckm* expression (*SI Appendix*, Fig. S3). Although KLF5 is necessary for the early stage of SC differentiation into myocytes, deletion of *Klf5* from myotubes by *Ckm-Cre* did not affect SC differentiation, as shown by the similar expression pattern of myogenic specification genes and myogenic markers (*SI Appendix*, Fig. S3). These results are consistent with the normal muscle development and function observed in cKO mice (*SI Appendix*, Fig. S2 *A–D*).

We found that Dex induced significant shortening of SC-derived myotubes but not a reduction in diameters (Fig. 2*B*). Dex clearly reduced levels of mRNAs encoding contractile proteins and concomitantly up-regulated expression of *Fbxo32* and *Trim63* mRNA, indicating Dex induced an atrophy-associated phenotype in SC-derived myotubes (Fig. 2*C*). It is therefore suggested that the shortening of myotube length is a morphological indicator of atrophy in this experimental model. Comparison of the responses to Dex of control and cKO myotubes showed that Dex-induced atrophy indicated by changes in morphology and mRNA expression were significantly suppressed in cKO myotubes (Fig. 2 *B* and *C*). This suggests KLF5 plays a key role in Dex-induced atrophy of SC-derived myotubes.

To investigate the mechanism by which *Klf5* deletion suppresses Dex-induced atrophy, we performed whole-transcriptomic analysis using RNA sequencing (RNA-seq). Interestingly, a majority of the genes differentially expressed in response to Dex were affected by *Klf5* deletion (Fig. 2 *D* and *E*). The genes down-regulated by Dex were divided into three major clusters based on K-means clustering. The genes in the clusters 1 and 2 were less down-regulated in cKO cells than control cells. Gene ontology analysis showed that the genes in clusters 1 and 2 were related to muscle actin filament–based process and vascular development, and their down-regulation is consistent with suppression of cKO cell atrophy (Fig. 2*D*).

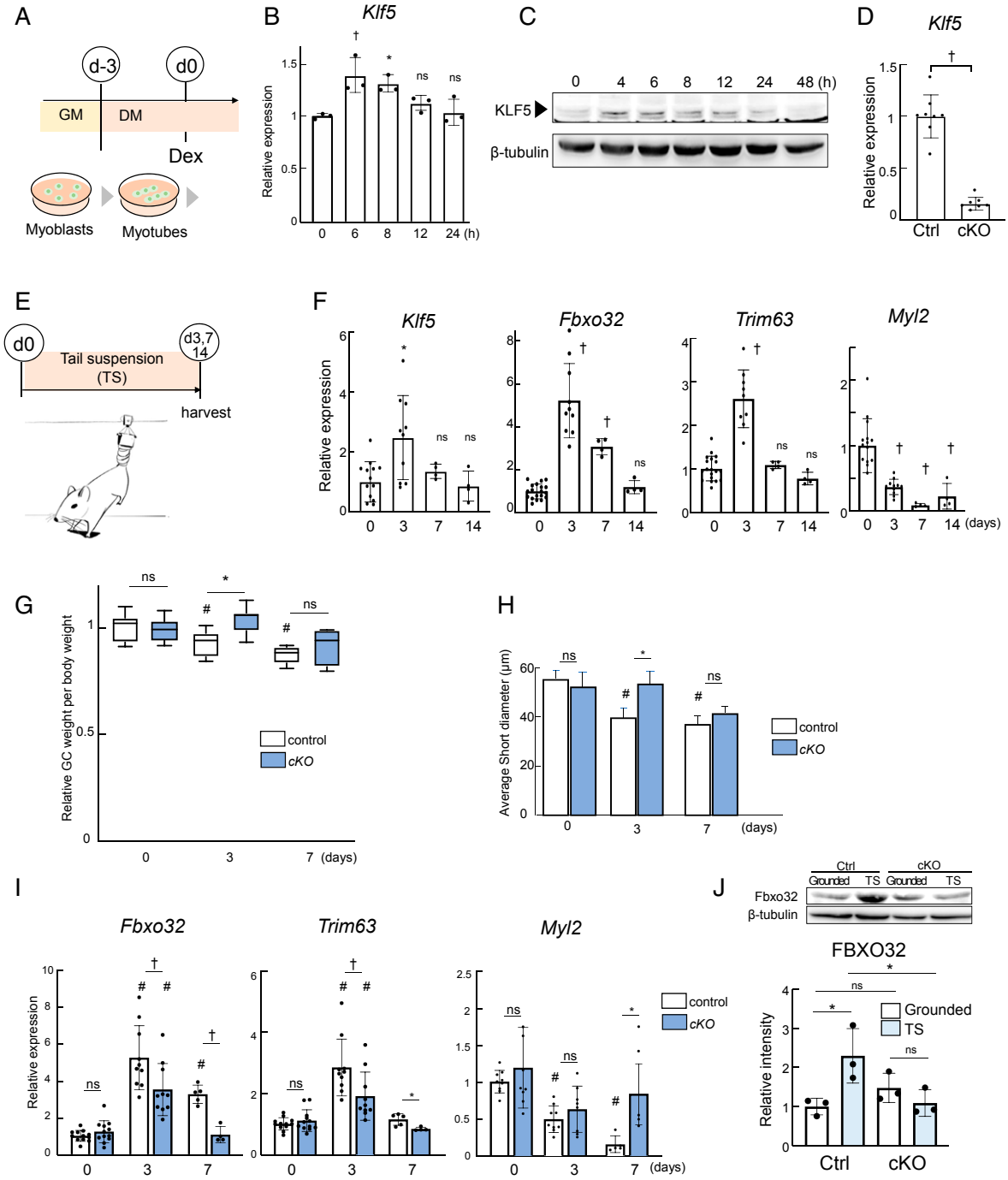

Fig. 1. KLF5 is important for muscle atrophy. (*A*) Scheme of the Dex-induced C2C12 myotube atrophy model. GM: growth medium, DM: differentiation medium. (*B*) *Klf5* mRNA expression in myotubes after Dex treatment. Data represent means ± SD, $n = 3$; one-way ANOVA and Dunnett's test for multiple comparisons versus 0 h. $^{*}P < 0.05$, $^{\dagger}P < 0.01$. ns, not significant. (*C*) KLF5 protein expression in myotubes exposed to Dex for the indicated times. Images are a representative of three samples showing similar results. (*D*) *Klf5* mRNA expression in gastrocnemius muscle before TS. Data represent means ± SD, $n = 7$ independent experiments; unpaired two-tailed Student's *t* test. $^{\dagger}P < 0.01$. (*E*) Scheme of the TS muscle atrophy model. Control $Klf5^{flox/flox}$ (Ctrl) and cKO mice were suspended by their tails for 3, 7, or 14 d (TS) and compared with the mice freely moving on the ground (Grounded). (*F*) *Klf5*, *Fbxo32*, *Trim63*, *and Myl2* mRNA expression after TS. Data are means ± SD $n = 4$ to 20 in each group, one-way ANOVA and Dunnett's test for multiple comparisons. $^{*}P < 0.05$, $^{\dagger}P < 0.01$ versus day 0. ns, not significant. (*G*) Box plots show the median, the 25th and 75th percentiles, and the range of values. Values were normalized to that on day 0 for the same genotype. $n = 5$ to 9 mice in each group; one-way ANOVA followed by Tukey's post hoc test for multiple comparisons. $^{\#}P < 0.05$ versus day 0 for the same genotype. $^{*}P < 0.05$ between genotypes on the same day. ns, not significant. (*H*) Average short diameter of muscle fibers in gastrocnemius muscle after 0, 3, or 7 d of TS. One thousand myofibers per group were randomly counted. Data are means ± SD $n = 5$ to 9 mice in each group; one-way ANOVA followed by Tukey's post hoc test for multiple comparisons. $^{*}P < 0.05$ versus control on the same day, $^{\#}P < 0.05$ versus day 0 for the same genotype. (*I*) *Fbxo32*, *Trim63*, and *Myl2* mRNA expression. Data are means ± SD $n = 9$ to 11 in each group; one-way ANOVA and Tukey's test for multiple comparisons. $^{*}P < 0.05$ versus control on the same day, $^{\#}P < 0.05$ versus day 0 for the same genotype. (*J*) Western blots of FBXO32 and β-tubulin in Ctrl and cKO gastrocnemius muscles from mice suspended for 3 d. Images are representative of three samples showing similar results. Relative band intensities corresponding to FBXO32 are shown in the bar graph. $n = 3$. One-way ANOVA and Tukey's test for multiple comparisons. $^{*}P < 0.05$, ns, not significant.

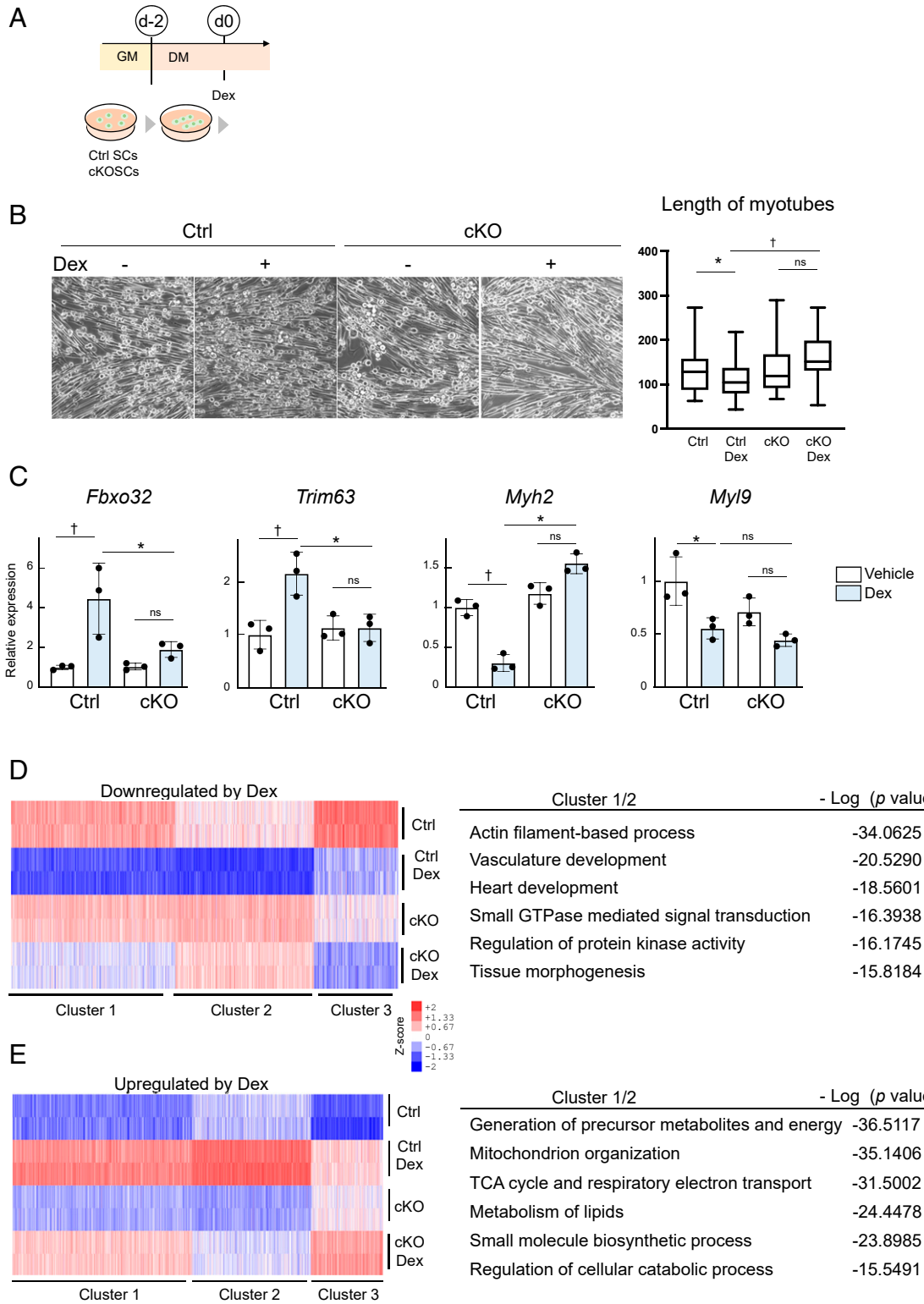

Fig. 2. KLF5 is required for Dex-induced atrophy-related gene regulation. (*A*) Scheme of the Dex-induced SC myotube atrophy model. GM, growth medium. DM, differentiation medium. SCs, satellite cells. (*B*) *Left*: phase contrast images of SC-derived myotubes treated with or without Dex for 48 h. *Right*: length of myotubes. Boxes show the means and the 25th and 75th percentiles; whiskers show the range of values; one-way ANOVA and Tukey's test for multiple comparisons. $^{*}P < 0.05$, $^{\dagger}P < 0.01$. ns, not significant. (*C*) *Fbxo32*, *Trim63*, *Myh2*, and *Myl9* mRNA expression in SC myotubes 24 h after Dex. Data are means ± SD $n = 3$; one-way ANOVA and Tukey's test for multiple comparisons. $^{*}P < 0.05$, $^{\dagger}P < 0.01$. ns, not significant. (*D* and *E*) Heatmaps showing expression levels of the genes down-regulated (*D*) or up-regulated (*E*) by 24 h of Dex treatment. RNA-seq read counts were analyzed using DESeq2 (64). Genes whose rlog counts were higher than eight in at least one sample and whose expression levels were significantly (FDR < 0.05) affected by Dex in Ctrl SCs were identified as differentially expressed genes and analyzed further. Dex induced up-regulation of 1,470 genes and down-regulation of 1,463 genes. The genes were divided into three groups based on K-means clustering. The top six enriched gene ontology terms for clusters 1 and 2 genes are also shown.

Likewise, *Klf5* deficiency suppressed induction of the majority of Dex–up-regulated genes (clusters 1 and 2 in Fig. 2*E*). The up-regulated genes belonging to clusters 1 and 2 included genes related to metabolism, such as energy metabolism and catabolism. This wide-spread induction of metabolism-related genes by Dex is consistent with earlier reports (22). It thus appears that *Klf5* deletion from myotubes suppresses Dex-induced changes in various genes, including metabolism-related genes and in turn myotube atrophy.

KLF5 Regulates Dex-Induced *Fbxo32* Transcription in Concert with Foxo1. To further investigate the KLF5-mediated program that governs muscle atrophy, we analyzed accessible chromatin regions globally using an assay for transposase-accessible chromatin-sequencing (ATAC-seq) with myotubes treated with Dex. After wild-type SC-derived myotubes were treated with Dex for 24 h, ATAC-seq peaks indicating that the loci opened in response to Dex were most highly enriched in motifs of two muscle lineage–determining transcription factors, MyoD and MEF2A, followed by Fos, which is known to be involved in the development of atrophy (Fig. 3*A*) (27, 28). In addition, binding motifs for KLF5 and Foxo1 ranked 8th and 16th, respectively (Fig. 3*A*). The accessible regions opened in response to Dex (identified using ATAC-seq) were enriched for genes associated with aspects of muscle structure and metabolism, such as actomyosin structure organization, contractile fibers, and abnormal gluconeogenesis (*SI Appendix*, Table S1). This highlights the effects of Dex on muscle structural and metabolism-related genes.

KLF5 often works together with other transcription factors. We previously reported that KLF5, MyoD, and Mef2 cooperate to drive transcription during myogenic differentiation (16). The Foxo family of transcription factors have been shown to promote diabetes-related muscle atrophy by inducing *Fbxo32* and *Trim63* (6, 22, 29). Based on those earlier findings, we hypothesized that KLF5 and Foxo1 may cooperate to mediate muscle atrophy. Because *Fbxo32* expression was decreased in *Klf5* knockout muscle and myotubes, we investigated *Fbxo32* as a potential target of KLF5 and Foxo1. Our previous chromatin immunoprecipitation sequencing (ChIP-seq) (GSE 80812) showed that in unstimulated C2C12 myotubes KLF5 binds to multiple sites in the *Fbxo32* gene locus along with MyoD (Fig. 3*B*). We then looked at the changes in KLF5 and Foxo1 binding to an enhancer of *Fbxo32* following 8 h of treatment with Dex. ChIP-qPCR clearly showed augmented association of KLF5 and Foxo1 with the enhancer within intron 4 of *Fbxo32* (GeneHancer identifier: GH08J123534), which has relatively conserved sequences across Euarchontoglires, including mice and humans, and contains putative binding motifs for KLF5 and Foxo1 (Fig. 3*C* and *SI Appendix*, Fig. S4*A*). Luciferase reporter analyses showed that while KLF5 and Foxo1 each transactivated the *Fbxo32* promoter alone, together they transactivated the promoter to a greater degree (*SI Appendix*, Fig. S4*B*). Moreover, coimmunoprecipitation experiments showed that KLF5 and Foxo1 directly interact with each other (Fig. 3*D*). The results indicate that in Dex-treated myotubes, KLF5 induces *Fbxo32* expression in concert with Foxo1.

Although the level of *Fbxo32* expression was significantly lower in cKO than control cells 24 h after Dex administration (Fig. 2*C*), KLF5 protein was detectable at that time, but its expression level was declining (Fig. 1*C*), which suggests the early induction of KLF5 may still affect *Fbxo32* transcription after 24 h (Fig. 3*C*). To address this possibility, we looked at the acetylation of histone H3 lysine 27 (H3K27ac), a dynamic histone modification that correlates with enhancer activity (30), around the *Fbxo32* promoter/enhancers. Eight hours after Dex in control cells, levels of H3K27ac at the *Fbxo32* promoter/enhancers were clearly elevated, indicating their activation (*SI Appendix*, Fig. S4*C*). By 24 h, H3K27ac levels had decreased but remained modestly increased at the intron 4 enhancer and proximal promoter. In cKO cells, the Dex-responsive induction of H3K27ac was much suppressed, and H3K27ac levels had returned to baseline by 24 h (*SI Appendix*, Fig. S4*C*). These findings demonstrate that KLF5 is essential for the activation of the *Fbxo32* enhancers and promoter in response to Dex. In addition, the early KLF5-mediated epigenetic modification at the enhancers and/or the remaining KLF5 protein appear to be important for the persistently activated states of the promoter and enhancer.

The KLF5 Inhibitor Am80 Attenuates Dex-Induced Muscle Atrophy. Am80, a synthetic RAR agonist, was shown to inhibit KLF5 activity and expression (17–19). Given that KLF5 is required for the muscle atrophy program, we hypothesized that inhibiting KLF5 using Am80 may prevent muscle atrophy. To test that idea, C2C12 myotubes were incubated for 24 h with Dex in the presence or absence of Am80 (Fig. 3*E*). Am80 suppressed the Dex-induced reduction in the myotube diameter (Fig. 3*F*). Am80 also attenuated Dex-induced expression of *Fbxo32* at both the mRNA and protein levels (Fig. 3 *G* and *H*) as well as the reduction in the expression of contractile protein genes exemplified by *Myh2* (Fig. 3*G*). Mechanistically, we found that the recruitment of KLF5 and Foxo1 and acetylation of H3K27 at the *Fbxo32* intron 4 enhancer were significantly reduced by Am80 treatment (Fig. 3*C*). Acetylation of H3K27 at the *Fbxo32* proximal promoter and 3′ enhancer were also decreased by Am80 (*SI Appendix*, Fig. S4*D*). *Fbxo32* promoter activity was also decreased by Am80 in reporter assays (*SI Appendix*, Fig. S4*B*). These observations demonstrate that Am80 suppresses Dex-induced *Fbxo32* activation at least in part by inhibiting the cooperative KLF5 and Foxo1 binding to and activation of the *Fbxo32* enhancer.

Am80 Protects Muscle From Disuse Atrophy. The observation that Am80 effectively suppressed the progression of Dex-induced atrophy in vitro led us to further test its potential against disuse atrophy. We first tested this idea in vitro using a three-dimensional (3D) clinostat apparatus, which can create a simulated microgravity (0.001 G) environment to induce myotube atrophy (Fig. 4*A*). After 48 h of simulated microgravity, C2C12 myotubes had become shortened in length but not diameter (Fig. 4*B*). This phenotypic change was accompanied by elevated mRNA expression of E3 ubiquitin ligases and *Klf5*, as well as decreased *Myl2* expression (Fig. 4*C*), indicating that clinorotation induces atrophy.

Having confirmed that the simulated microgravity induces atrophy in C2C12 myotubes, we examined the effect of Am80. Addition of Am80 to the culture medium suppressed the shortening of myotubes (Fig. 4*B*), and there was a corresponding cancelation of the decrease in *Myl2* mRNA otherwise seen (Fig. 4*C*). Importantly, Am80 significantly inhibited the induction of *Klf5*, *Fbxo32*, and *Trim63* mRNA (Fig. 4*C*), and Western blotting indicated that Am80 also suppressed the induction of FBXO32 protein (Fig. 4*D*). These results demonstrate that Am80 inhibits the atrophy program otherwise activated in myotubes in response to simulated microgravity.

To test whether Am80 would inhibit unloading-mediated muscle atrophy in vivo, wild-type C57BL/6 male mice were orally administered Am80 (3.0 mg/kgBW/day) or vehicle (dimethyl sulfoxide [DMSO]) daily. Administration was started 1 d before and continued throughout the TS (Fig. 4*E*). No significant changes in body weight were observed during the test period (*SI Appendix*, Fig. S5*A*). After 3 d of unloading, gastrocnemius muscle weight was significantly reduced in the vehicle-treated mice but not the Am80-treated mice (Fig. 4*F*). Am80 attenuated the induction of *Fbxo32* and *Trim63* mRNA as well as the reduction in *Myl2* mRNA (Fig. 4*G*). Moreover, Western blotting confirmed that Am80 decreased expression of FBXO32 protein in the atrophied muscle (Fig. 4*H*).

We next investigated whether Am80 would ameliorate the longer-term, unloading-mediated muscle atrophy. Administration

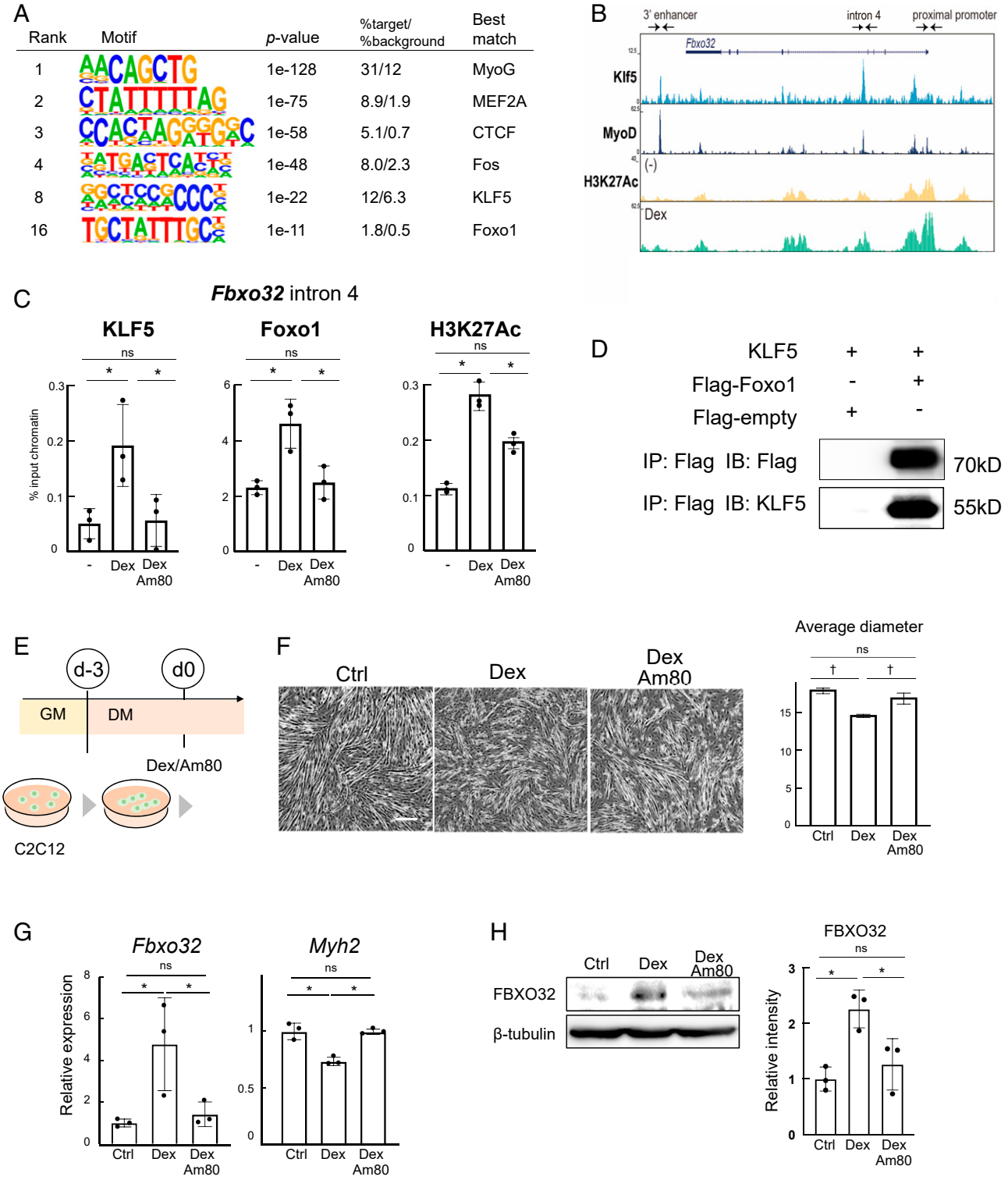

Fig. 3. KLF5 controls *Fbxo32* transcription in concert with Foxo1 and is inhibited by Am80. (*A*) De novo motifs identified in the chromatin regions opened by Dex in SC-derived myotubes. (*B*) A University of California, Santa Cruz genome browser shot illustrating normalized tag counts for KLF5, MyoD, and H3K27Ac at the *Fbxo32* gene locus in C2C12 myotubes. Note that the H3K27Ac tag count around *Fbxo32* enhancers was increased after 8 h of Dex treatment. (*C*) ChIP-qPCR analysis of the association of KLF5, Foxo1, and H3K27Ac with the *Fbxo32* intron 4 enhancer after 8 h of Dex treatment. $*P < 0.05$. (*D*) Coimmuno-precipitation of Foxo1 with KLF5. Cell lysates from HEK293T cells transfected with mouse KLF5 expression vector, Flag-tagged mouse Foxo1 expression vecto,r or empty Flag vector were pulled down with anti-Flag antibody. (*E*) Experimental scheme for evaluating the effects of Dex on C2C12 myotubes with or without Am80 treatment. (*F*) *Left*: phase contrast images of C2C12 myotubes after 48 h of Dex exposure. *Right*: average diameter of myotubes. One hundred randomly selected myotubes were measured in each group; one-way ANOVA and Tukey's test for multiple comparisons. $^{\dagger}P < 0.01$. ns, not significant (Scale bar; 100 μm). (*G*) Expression of *Fbxo32* and *Myh2* mRNA in C2C12 cells after 12 h in Dex-containing medium with or without Am80. Data are means ± SD, $n = 3$ wells; one-way ANOVA and Tukey's test for multiple comparisons. $*P < 0.05$. ns, not significant. (*H*) FBXO32 protein expression at after 24 h of the indicated treatment. Images are representative of three samples. Relative band intensities corresponding to FBXO32 are shown in the bar graph ($n = 3$). $*P < 0.05$. ns, not significant.

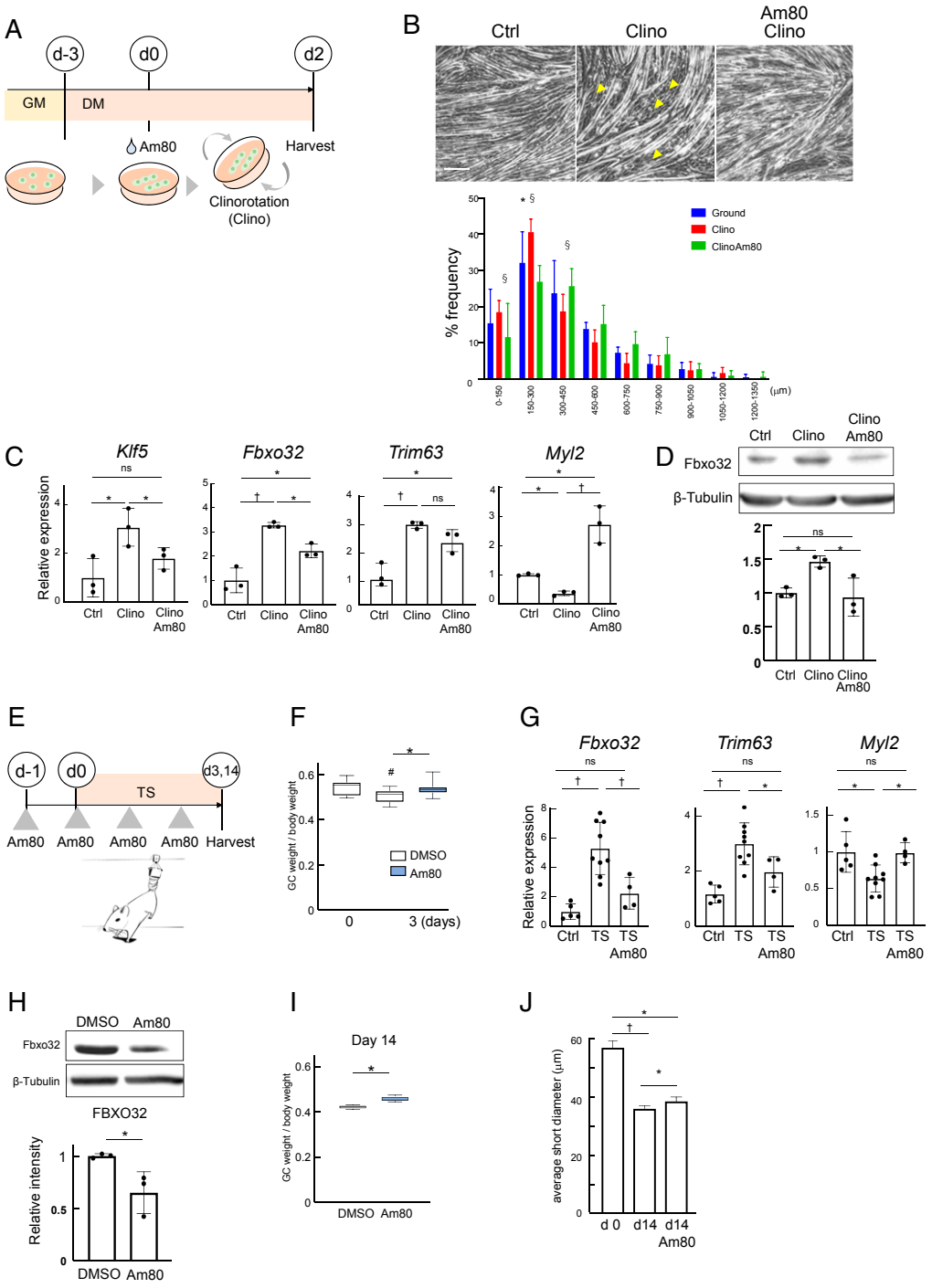

Fig. 4. Am80 rescued KLF5-mediated unloading atrophy in vitro and in vivo. (*A*) Scheme for induction of atrophy by simulating microgravity (0.001 G) using clinorotation (Clino). (*B*) Phase contrast images of C2C12 myotubes after 48 h of microgravity with or without Am80. *Bottom*: distribution of myotube lengths. Data are means ± SD. Mean numbers of myotubes within the indicated length ranges per 100 myotubes/experimental condition are shown; one-way ANOVA and Tukey's test for multiple comparisons. $*P < 0.05$ ground versus clino, $^{\S}P < 0.05$ clino versus Am80 (Scale bars, 100 μm). (*C*) Expression of *Klf5*, *Fbxo32*, *Trim63*, and *Myl2* mRNA in C2C12 myotubes cultured with or without clinorotation ($n = 3$). $*P < 0.05$, $^{\dagger}P < 0.01$, ns, not significant. (*D*) FBXO32 protein in C2C12 myotubes cultured under clinorotation with or without Am80. Relative band intensities corresponding to FBXO32 are shown in the bar graph ($n = 3$). (*E*) Experimental schedule for oral Am80 administration and TS. (*F*) Gastrocnemius (GC) weight per body weight (BW) after TS with Am80 administration. Box plots show the median, 25th and 75th percentiles, and range of values. n =11 to 21 in each condition; one-way ANOVA and Tukey's test for multiple comparisons. $^{\#}P < 0.05$ versus day 0, $*P < 0.05$ between treatments on the same day, ns, not significant. (*G*) *Fbxo32*, *Trim63*, and *Myl2* mRNA expression in gastrocnemius muscle after 3 d of TS with or without Am80. Data are means ± SD $n = 4$ to 8; one-way ANOVA and Tukey's test for multiple comparisons. $*P < 0.05$, $^{\dagger}P < 0.01$, ns, not significant. (*H*) FBXO32 protein expression after 3 d of TS. Images are representative of three samples. Relative band intensities corresponding to FBXO32 are shown in the bar graph. Student's two-tailed t test. $*P < 0.05$. (*I*) Gastrocnemius (GC) weight per body weight (BW) after TS with Am80 administration for 14 d. Box plots show the means, 25th and 75th percentiles, and range of values. $n = 5$ per group, unpaired two-tailed Student's t test. $*P < 0.05$. (*J*) Average short diameter of muscle fibers in the gastrocnemius muscle following 14 d of TS. One thousand myofibers per group were randomly counted. Data are means ± SD $n = 3$ mice per group; one-way ANOVA and Tukey's test for multiple comparisons. $*P < 0.05$, $^{\dagger}P < 0.01$.

of Am80 throughout the 14-d unloading period modestly but significantly suppressed the reductions in gastrocnemius mass (Fig. 4*I*). Shortening of the average fiber diameter on day 14 was also suppressed by administration of Am80, whereas there was no significant difference after 3 or 7 d (Fig. 4*J* and *SI Appendix*, Fig. S5*B*).

We further examined whether Am80 would prevent Dex-induced atrophy, an often used in vivo muscle atrophy model (31). Dex injection for 5 consecutive d significantly decreased gastrocnemius muscle weight by 9.26% (*SI Appendix*, Fig. S6*A*), and the average short diameter was also significantly decreased after 5 d of Dex (*SI Appendix*, Fig. S6*B*). In this model, *Klf5*, *Fbxo32*, and *Trim63* mRNA levels were significantly increased on day 3 and reached a peak on day 5 after starting Dex (*SI Appendix*, Fig. S6*C*). In the Am80-treated group, Dex-induced shortening of myofiber diameters was significantly attenuated (*SI Appendix*, Fig. S6*B*) and was accompanied by diminished *Fbxo32* and *Trim63* induction on day 5 (*SI Appendix*, Fig. S6*D*). These findings demonstrate that oral Am80 protects mice from muscle atrophy caused by unloading or Dex.

Human Muscle Atrophy Is Associated with *KLF5* Expression. Finally, we asked whether KLF5 was involved in human sarcopenia. To address that question, we analyzed three publicly available datasets from RNA-seq analyses from human muscle samples (GSE113165, GSE129643, and GSE111017). Mahmassani et al. analyzed the effects of 5 d of bedrest on the transcriptome of the vastus lateralis muscle (32). In that dataset (GSE113165), we noted that levels of *KLF5* expression tended to be increased by bedrest ($P = 0.0502$) (*SI Appendix*, Fig. S7*A*) and were higher in muscles of aged subjects than young subjects (*SI Appendix*, Fig. S7*B*). Moreover, levels of *KLF5* expression correlated with those of *FBXO32* and *TRIM63* expression (*SI Appendix*, Fig. S7*C*). Consistent with those findings, *KLF5* expression correlated with age in a separate RNA-seq dataset (GSE129643) from muscle samples from healthy individuals of various ages (*SI Appendix*, Fig. S7*C*) (33). In that gene set and an additional gene set that analyzed the transcriptomes in muscle samples from healthy elderly subjects with or without sarcopenia (GSE111017) (34), *KLF5* expression levels correlated with those of *FBXO32* and *TRIM63* (*SI Appendix*, Fig. S7 *D* and *E*). These results indicate that *KLF5* expression associates with *FBXO32* and *TRIM63* expression in human muscle. *KLF5* expression thus appears to be positively correlated with age-related muscle atrophy in humans. Levels of *Klf5* and *Fbxo32* expression were also higher in gastrocnemius muscles from aged (2 y old) mice than from young (8 wk old) mice (*SI Appendix*, Fig. S8). *Trim63* expression tended to be similarly increased, but the difference did not reach statistical significance. These mouse results corroborate the age-associated up-regulation of *Klf5* in muscles.

Discussion

Muscle atrophy is caused by a combination of multiple factors, including malnutrition and mechanical unloading or disuse. The results of this study demonstrated the essential role of KLF5 in the control of muscle atrophy. First, KLF5 is indispensable for induction of E3 ubiquitin ligases and muscle atrophy caused by Dex and microgravity, which mimic unloading in vitro. Second, muscle-specific deletion of *Klf5* rescued hind-limb muscles from atrophy caused by unloading. Third, administration of a KLF5 inhibitor, Am80, attenuated muscle atrophy in vitro and in vivo.

KLF5 has multiple functions in skeletal muscle. It is an important regulator of skeletal muscle regeneration that acts by regulating muscle-specific genes in cooperation with MyoD and MEF2 (16). In addition, KLF5 controls fatty acid metabolism in adult skeletal muscle in cooperation with PPAR-δ (15). In those settings, KLF5 interacts with various transcription factors and coregulators. In the present study, we found that KLF5 physically interacts with Foxo1, with which it acts cooperatively to control *Fbxo32* transcription (Fig. 3 *B–D*). Our results highlight the notion that its combinatorial interactions with other transcription factors enable KLF5 to control different sets of genes in a context-dependent manner in skeletal muscle. It is noteworthy that by using a *Pax7*-CreER system, which enabled deletion of *Klf5* in undifferentiated myoblasts, we were able to show that KLF5 is necessary for early differentiation of myotubes. In the present study, we used *Ckm*-driven Cre. *Ckm* expression was low at the myoblast stage and was induced beginning 1 d after SC differentiation had started (*SI Appendix*, Fig. S3). Consequently, *Klf5* expression was efficiently repressed beginning 2 d after the onset of differentiation in SCs, and myotube differentiation was not affected (*SI Appendix*, Fig. S3). Given that no obvious abnormalities were observed in the muscle mass, histology, fiber type, or function in skeletal muscle in cKO mice (*SI Appendix*, Fig. S2 *A–D*), it is likely that *Klf5* was deleted from cKO mice only after the early muscle differentiation processes that depend on KLF5 had been completed.

The present study also shows that Am80 efficiently suppresses Dex- and microgravity-induced muscle atrophy in vitro and disuse-induced muscle atrophy in mice in vivo. It was previously reported that retinoids enhance myoblast differentiation and muscle repair after injury and modulate lipid metabolism in myocytes, which suggests they may exert beneficial effects mitigating muscle atrophy (35–41). This study shows that a retinoid could successfully prevent muscle atrophy. Am80 was previously shown to inhibit KLF5 through at least two mechanisms: disruption of the KLF5/RAR/RXR complex and inhibition of *Klf5* expression (42, 43). Am80 suppressed binding of KLF5 to the *Fbxo32* enhancer and inhibited its activation by Dex (Fig. 3*B*). Importantly, Am80 simultaneously decreased Foxo1 binding to the *Fbxo32* enhancer, suggesting Am80 impairs formation of a transactivation complex on the enhancer. Although our motif analysis of Dex-opened chromatin regions did not identify an RAR motif, unliganded RAR can act as a coactivator of KLF5 at the site without a clear RAR binding motif (17–19). It is therefore possible that RAR is involved in regulating *Fbxo32* and other atrophy-related genes, though characterization of the regulatory role of RAR and the global epigenetic effects of RAR agonists, such as Am80, during muscle atrophy awaits further study.

Retinoic acid agonists may exert beneficial effects preventing sarcopenia through multiple mechanisms in addition to inhibiting the KLF5-dependent muscle atrophy program. RAR agonists promote muscle regeneration after injury, at least in part by suppressing differentiation and promoting apoptosis of fibro/adipogenic progenitor cells that lead muscle fibrosis and regeneration (40, 41). Retinoids may also affect SC quiescence and differentiation. Stimulation of retinoic acid signaling inhibits differentiation of mouse SCs and human myoblasts, keeping them in an immature state (36). A major portion of quiescent SCs in aged mice express a cellular senescence marker, $p16^{INK4a}$ (CDKN2A), and exhibit impaired regeneration capacity due in part to their failure to enter the cell cycle upon activation (44, 45). Because greater numbers of cell cycles may induce DNA damage that drives cellular senescence (46, 47), retinoid-mediated maintaining SC quiescence may be beneficial to maintaining a functional SC pool. In that regard, chronic inflammation has been shown to promote cellular senescence and stem cell dysfunction (46), and retinoids have anti-inflammatory and immunomodulatory properties (48). It will be important to analyze the effects of retinoids on SC dysfunction in aging muscle. In addition, sarcopenia often occurs in conjunction with various age-associated pathologies, including osteopenia/osteoporosis and cardiovascular diseases. Activation of RAR signaling has been shown to be beneficial in various age-associated diseases (49), making retinoids attractive drug candidates for patients exhibiting multimorbidity.

Several KLF members have been shown to have various functions in skeletal muscle (13). For instance, a recent study revealed that KLF15 mediates hyperglycemia-induced skeletal muscle atrophy (50). KLF15 is a substrate of E3 ubiquitin ligase WWP1. Because WWP1 function is down-regulated by hyperglycemia, KLF15 accumulates within myocytes, resulting in atrophy. KLF15 is also induced by Dex in vitro and in vivo, and overexpression of *Klf15* up-regulates atrophy-related genes (51). In that study, KLF15 was shown to transactivate *Fbxo32*. However, conflicting data have also been reported (52) (i.e., moderate overexpression of *Klf15* in skeletal muscle did not induce muscle atrophy, and *Klf15* deletion did not affect chronic Dex-induced muscle atrophy). The role of KLF15 in Dex-induced muscle atrophy thus remains unclear. KLF5 is induced in response to Dex and unloading, whereas KLF15 is activated by hyperglycemia and possibly by Dex. This suggests the two may respond to different signals to regulate genes involved in muscle atrophy, including shared target genes, such as *Fbxo32*. And while both KLF5 and KLF15 control metabolic genes, they appear to play different roles in metabolic regulation. For instance, KLF15 is activated by fasting and promotes amino acid catabolism (53, 54). Because metabolic changes are integral to muscle atrophy, it will be important to elucidate the interactions among KLF members in muscle metabolism.

Previous studies showed that Foxo family members, including Foxo1 and Foxo3, regulate both the ubiquitin–proteasome system and the autophagy pathway during atrophy (6, 10, 55). Although Foxo1 and Foxo3 both belong to the Foxo transcriptional protein family and share overlapping structure and function, they harbor several important differences. Only systemic deletion of Foxo1 is embryonically lethal in mice (56), which implies the functions of Foxo1 are indispensable and cannot be compensated for by other Foxos. In the present study, we found that KLF5 directly interacts with Foxo1 but not Foxo3. However, this does not necessarily exclude the possibility that the KLF5-mediated atrophy program is affected by Foxo3. In fact, the transcriptional regulatory region of *Foxo1* contains a consensus Forkhead response element that is activated by Foxo3 (57).

Several human studies have demonstrated that *KLF5* expression is higher in muscles of aged subjects than young subjects (33, 58). Similarly, the level of Klf5 expression was higher in muscles of aged (2 y old) mice than young (8 wk old) mice (*SI Appendix*, Fig. S8). Using three publicly available datasets, we also found that *KLF5* expression increases with age, the level of *KLF5* expression is positively associated with those of *FBXO32* and *TRIM63*, and *KLF5* expression tends to be increased after the bedrest (*SI Appendix*, Fig. S7). These results, along with our finding that KLF5 is important for regulation of atrophy-related genes (e.g., *Fbxo32* and *Trim63*) in models of physical inactivity (TS) and metabolic alteration (Dex), suggest that KLF5 may also be involved in the pathogenesis of disuse-induced muscle atrophy in humans. However, human disuse muscle atrophy is often caused by longer and/or repetitive physical inactivity. Moreover, sarcopenia is likely to involve multiple factors that include both physical and metabolic alterations. Accordingly, more studies are clearly needed to elucidate the precise roles of KLF5 in human muscle atrophy and sarcopenia.

In summary, our present study indicates that KLF5 is an important regulator of muscle atrophy caused by unloading and DEX administration in mice. Although a variety of candidate drugs, including myostatin/ActR2 signaling inhibitors, exercise mimetics, anabolic hormones, and natural compounds, are under investigation, no therapeutic strategy or medication for sarcopenia has yet been established. Our findings demonstrate that a KLF5 inhibitor, Am80, protects mouse muscle from atrophy. As Am80 is already approved for clinical use in the treatment of promyelocytic leukemia (59), its safety and stability are established. We therefore suggest that pharmacological intervention with Am80 is a potentially effective means of preventing muscle atrophy.

Materials and Methods

Antibodies. For Western blotting, rat anti-KLF5 (16), mouse anti-Atrogin-1 (MAFbx (F-9): sc-166806, Santa Cruz), mouse anti-MuRF1 (MuRF1(C-11): sc-398608, Santa Cruz), and mouse anti-beta-tubulin (Wako) antibodies were used. For ChIP-PCR, anti-Foxo1 (Abcam, ab39670) and anti-H3K27Ac (Abcam, ab4729) were used.

Mice. C57BL/6J (WT) mice were purchased from Sankyo Labo Service. *Klf5$^{flox/flox}$* (Ctrl) mice (Jackson Laboratory, 029787) were bred with *Ckm-Cre* mice (25) to generate *Ckm-Cre;Klf5$^{flox/flox}$* (cKO) mice. Seven- to nine-week-old male Ctrl and cKO mice were randomized into groups for oral administration of Am80 or DMSO.

All mice were housed in a temperature- and humidity-controlled room with a 12-h light/dark cycle. All animal experiments were approved by the Institutional Animal Care and Use Committee and Genetically Modified Organisms Safety Committee of Tokyo Medical and Dental University (Approval No. 0170317A and 2015-007C, respectively) and conducted in accordance with the guidelines concerning the management and handling of experimental animals.

Am80 Administration. Am80 was synthesized as described previously (60) and was initially prepared in a 10 mmol/l stock solution in DMSO and then further diluted with saline. Oral administration of Am80 (3.0 mg/kg/day) or vehicle alone to mice was commenced 1 d prior to TS and then continued for 3 d during TS.

TS. The TS device was from Takatsuka Life Science. To induce hind limb muscle atrophy, Ctrl and cKO mice were held by their tails in a fixed position with adhesive tape to ensure that their hind legs could not touch the ground. They could move freely within their cage using their forelimbs and accessed their food just as control mice did. After suspension for 3, 7, or 14 d, the gastrocnemius and soleus muscles were harvested.

Cell Culture. C2C12 mouse skeletal muscle cells (American Type Culture Collection; ATCC No. CRL-1772, passage numbers 6 to 8) were cultured at 37 °C under 5% CO_2 in Dulbecco's modified Eagle medium (DMEM; NACALAI TESQUE, INC.) supplemented with 10% fetal bovine serum (FBS; GE Healthcare Life Science) and 1% penicillin-streptomycin (NACALAI TESQUE, INC.). Cells were passaged every 3 d. To induce differentiation, when cells reached about 90% confluence, the growth medium was replaced with differentiation medium composed of DMEM supplemented with 2% horse serum (GE Healthcare Life Science) and 1% penicillin-streptomycin. After differentiation for 3 d, C2C12 myotubes were treated with 10 μM DEX and/or 100 nM Am80 for the indicated times.

Plasmid Vectors and Transfection. pFlag-CMV2-mouse Foxo1 expression plasmid was a generous gift from Dr. Nakae (International University of Health and Welfare, Narita, Japan), and pGL3-Fbxo32 promoter luciferase plasmid was a generous gift from Dr. Lecker (Beth Israel Deaconess Medical Center, Boston, MA). The plasmids were transfected into C2C12 cells using Lipofectamine 2000 reagent (Thermo). At 24 h after transfection, total cell lysates were collected and subjected to immunoprecipitation.

SC Isolation, Culture Conditions. Mouse primary SCs were isolated from hindlimb muscles from male *Ckm-Cre;Klf5$^{flox/flox}$* and control (*Klf5$^{flox/flox}$*) mice. After excess fat, connective tissue, and tendons were removed, hindlimb muscles were minced and digested in 0.2% collagenase type II (Worthington Biochemical Corp.) for 1 h at 37 °C. Mononuclear cells were stained with PE-Cy7–conjugated anti-CD31, -CD45, and -Ly6A/E as well as fluorescein isothiocyanate (FITC)-conjugated anti-CD106 antibodies for 30 min on ice and resuspended in phosphate buffered saline (PBS) containing 2% FBS. SCs were isolated using a fluorescence-activated cell sorting (FACS) Aria III flow cytometer (BD Biosciences). Debris and dead cells were excluded by forward scatter, side scatter, and 7-AAD gating. Data were collected using FACS Diva software and FlowJo (BD Biosciences). SCs were cultured in GlutaMax DMEM (Life Technologies) supplemented with 20% FBS, 10 ng/mL basic fibroblast growth factor (Cell Signaling Technology, Beverly, MA), 0.2 μg/cm^2 iMatrix-511 silk (Takara bio), and 1% penicillin-streptomycin at 37 °C under 5% CO_2. Myogenic differentiation was induced in GlutaMax DMEM supplemented with 5% horse serum and 1% penicillin-streptomycin on Matrigel-coated plate at 37 °C under 5% CO_2.

3D-Clinorotation Culture. Microgravity conditions were produced using a 3D-Clinorotation apparatus (Gravite, Space Bio-Laboratories Co., Ltd.) as

MEDICAL SCIENCES

descried previously (61). This device produces an environment similar to that of outer space (0.001 G) by rotating a sample around two axes, integrating a gravity vector with a temporal axis. This is accomplished by rotation of a chamber at the center of the device, which results in uniform dispersion of the gravity vector within a spherical volume, with a constant angular velocity. Within 8 min, these conditions produced a simulated environment of 10^{-3} G, measured with a gravity acceleration sensor, which was defined as simulated microgravity. Differentiated C2C12 myotubes were cultured in a cell culture flask (T-75, Corning) with or without 100 nM Am80 for 48 h in the simulated microgravity at 37 °C. As a control, C2C12 myotubes in the same cell culture flask were cultured under the ground conditions at 37 °C.

RT-PCR Analysis. Total RNA from cultured cells or mouse tissue was isolated using ISOGEN (NIPPON GENE) according to the manufacturer instructions. Complementary DNA (cDNA) was synthesized using ReverTra Ace qPCR RT Master Mix with genomic DNA (gDNA) Remover (TOYOBO CO., LTD.). All qPCR protocols were performed with StepOne Plus (Applied Biosystems) using a KAPA SYBR FAST ABI Prism qPCR Kit (KAPA BIOSYSTEMS). Primers are listed in *SI Appendix*, Table S2.

RNA-Seq. Total RNA was isolated and purified using RNeasy columns and RNase-free DNase digestion according to the manufacturer's instructions (QIAGEN). Poly-A mRNA was extracted from total RNA using Oligo-dT beads in a NEBNext Poly(A) RNA Magnetic Isolation Module (New England Biolabs), after which RNA-seq libraries are prepared using an RNA-Seq library preparation kit for Illumina (New England Biolabs) according to the manufacturer's protocols. Libraries were single-end sequenced on a Hiseq1500 sequencer (Illumina). Reads were aligned with the mm9 mouse genome using STAR (62). Aligned read files were analyzed using HOMER (63). Differentially expressed genes were analyzed using DESeq2 (64). Gene set analysis was performed using Metascape (65). K-means clustering was performed using Cluster 3.0.

For analysis of publicly available human RNA-seq datasets, FASTQ files were downloaded from the Gene Expression Omnibus (GEO). Reads were aligned with the hg38 human genome using STAR (62). Aligned read files were then analyzed using HOMER (63), after which transcripts per kilobase million values were calculated. GSE111017 contained data from three cohorts. Because initial analyses showed that expression levels of *KLF5* and other marker genes in one cohort (Jamaica Sarcopenia Study) diverged from the other two cohorts (Hertfordshire Sarcopenia Study and Singapore Sarcopenia Study), we used the data from the latter two cohorts for further analyses.

ChIP. For ChIP-qPCR, 1×10^7 C2C12 cells were used. Briefly, the cells were crosslinked in 2 mM disuccinimidyl glutarate (Thermo Fisher) and 1% formaldehyde, after which they were collected and resuspended for 5 min in swelling buffer (10 mM Hepes/KOH pH 7.9, 85 mM KCl, 1 mM ethylenediamine tetraacetic acid [EDTA], 0.5% IGEPAL CA-630) containing protease inhibitors. The cells were then spun down and resuspended in 500 μL lysis buffer (50 mM Tris/HCL pH 7.4, 1% sodium dodecyl sulfate [SDS], 0.5% Empigen BB, 10 mM EDTA) containing protease inhibitors, and chromatin was sheared by sonication. The lysate was diluted with 750 μL dilution buffer (20 mM Tris/HCl, 100 mM NaCl, 0.5% TritonX-100, 2 mM EDTA), after which 1% was taken as input DNA, and immunoprecipitation was carried out overnight using Dynabeads protein G (Thermo Fisher) coated with specific antibody. Thereafter, the beads were washed two times each with wash buffer I (20 mM Tris/HCl, 150 mM NaCl, 0.1% SDS, 1% Triton X-100, 2 mM EDTA), wash buffer II (10 mM Tris/HCl, 250 mM LiCl, 1% IGEPAL CA-630, 0.7% Na-deoxycholate, 1 mM EDTA), TE plus 0.2% triton X-100, and TE plus 50 mM NaCl and then eluted with elution buffer (TE, 2% SDS). DNA was reverse crosslinked and purified using a QIAquick PCR purification Kit (Qiagen) according to the manufacturer's instructions.

ATAC-Seq Library Preparation. Approximately 50,000 cells were washed once with PBS and once with cold lysis buffer (10 mM Tris HCl, pH 7.4, 10 mM NaCl, 3 mM MgCl2, 0.1% IGEPAL CA-630). The cells were then suspended in 50 μL 1× reaction buffer (25 μL Tagment DNA Buffer, 2.5 μL Tagment DNA enzyme I, and 22.5 μL water) (Nextera DNA Library Preparation Kit, Illumina) as previously described (66). Transposase reactions were carried out at 37 °C for 30 min, and the DNA was immediately purified using a PCR purification Kit (Qiagen). The DNA was amplified for 14 cycles using Nextera primer Ad1 and a unique Ad2.n barcoding primer with NEBNext High-Fidelity 2XPCR Master Mix (NEB). The resulting libraries were size selected, single-end sequenced using a HiSEq1500 sequencer (Illumina) for 51 cycles according to the manufacturer's instructions.

Reads were aligned with the mm9 mouse genome using STAR (62). Peak detection and de novo motif analysis were carried out using HOMER (63). Peaks that overlapped blacklisted regions (67) or simple repeat regions were removed. For identification of ATAC peaks affected by Dex, peaks detected in the control and Dex-treated samples were merged. To focus on potential enhancers, ATAC peaks in the vicinity of the transcription start and stop sites were removed. Counts within 200 base pair (bp) around the merged ATAC peaks were calculated and analyzed using DESeq2. The ATAC peaks with counts in the Dex samples that were more than twofold greater than those in the control samples were used as Dex-opened peaks and subjected to de novo motif analysis. ATAC-seq peaks, indicating loci opened in response to Dex, were analyzed using GREAT (68).

Immunoprecipitation. Immunoprecipitation of Flag-tagged proteins was performed using a FLAG Immunoprecipitation Kit (Sigma) according to the manufacturer's instructions. Briefly, differentiated C2C12 myotubes were lysed for 30 min in buffer containing 50 mM Tris HCl, 150 mM NaCl, 1 mM EDTA, and 1% Triton X-100. Aliquots of cell lysate containing 600 μg of whole-cell protein were mixed with washed ANTI-FLAG M2 affinity gel and incubated overnight at 4 °C. After the incubation, the samples were washed three times with 1× wash buffer (50 mM Tris HCl, 150 mM NaCl), and Flag-tagged protein was precipitated from SDS sample buffer by heating the sample to 98 °C for 5 min.

Western Blotting. Whole-cell protein was isolated using radioimmunoprecipitation assay (RIPA)-SDS buffer (5 M NaCl, 1 M Hepes, 20% Nonidet P-40, 10% sodium deoxycholate, 10% SDS, 0.5 M EDTA (pH 8.0)). Equal amounts of protein (30 μg/lane) were separated with SDS-polyacrylamide gel electrophoresis (PAGE) (10% Separating gel), transferred to polyvinylidene difluoride (PVDF) membranes, and blocked with 5% bovine serum albumin (Wako)/T-TBS for 1 h at room temperature. The membranes were then incubated first overnight at 4 °C with primary antibody and then for 1 h at room temperature with anti-rat IgG HRP-linked whole antibody (GE Healthcare) and anti-mouse IgG HRP-linked whole antibody (GE Healthcare). The signal was detected with ECL Prime Western Blotting Detection Reagent (GE Healthcare) according to the manufacturer's instructions. Each experiment was replicated at least three times.

Hematoxylin and Eosin (H&E) Staining. Soleus and gastrocnemius muscles were fixed by immersion in Tissue-Tek Ufix (Sakura finetek) and embedded in paraffin blocks. Then, 10-μm-thick sections were deparaffinized, rehydrated, stained with hematoxylin for 3 min, washed with running water for 15 min, stained in eosin for 15 min, quickly washed in a 70, 80, 90, 95, and 100% EtOH series, and finally washed twice in xylene and then examined by light microscopy. H&E-stained section of gastrocnemius was analyzed by CellSence software (Olympus Life Science). Muscle fiber diameters were measured in photomicrographs of H&E-stained muscle tissue sections. One thousand myofibers per condition were randomly counted, and the data are shown as mean size ± SD.

Measurement of the Diameter of C2C12 Myotubes and the Length of SC-Derived Myotubes. Images of myotubes were acquired using a phase contrast microscope (Olympus) and analyzed using Image J (NIH) and CellSence software (Olympus Life Science). Myotubes were defined as elongated structures containing three or more nuclei within a single membrane structure (69). Most myotubes were aligned to the uniaxial isometric lines of strain, but some singular branched dysmorphic myotubes were counted. Myotube diameters were calculated as the average of 10 measurements for a representative measure (70, 71). One hundred randomly selected myotubes per experimental condition were counted. To evaluate SC-derived myotubes, myotube length was calculated as the average of 10 measurements along the myotube length (72). One hundred randomly selected myotubes per experimental condition were counted. For all measurements, 3 to 6 images from at least three replicates were used.

Statistics and Reproducibility. Statistical analyses were performed using Graph Pad Prism 8 and 9 software and with Python using numpy and scipy. The images were prepared using Adobe Illustrator CS5 and Photoshop CS5.1 and with Python using matplotlib and seaborn. Heatmaps were generated using Java Treeview (73). Sample sizes were not based on power calculations. Data are presented as the mean ± SD, except where otherwise indicated. For experiments involving two factors, data were analyzed using two-way ANOVA followed by Tukey's or Dunnett's post hoc tests, except where otherwise indicated. Individual pair-wise comparisons were made using Student's *t* test, except where otherwise indicated. Values of $P < 0.05$ were considered significant.

Data Availability. All RNA-seq and ATAC-seq data are available in the GEO under Accession GSE165072. Our previous ChIP-seq results used in this study are also available (GSE80812). All other study data are included in the article and/or *SI Appendix*.

ACKNOWLEDGMENTS. We thank Noriko Yamanaka, Eriko Magoshi, and Kaori Ogasawara for their excellent technical assistance. This study was supported by Japan Society for the Promotion of Science (JSPS) KAKENHI Grants JP17K09589, JP17H05636, JP19K20178, JP20H03679, JP20H04956, JP20H04938, JP19H03648, JP20K21594, and JPMJMS2023 from Japan Science and Technology Agency (JST); by Japan Agency for Medical Research and Development (AMED) under Grants JP21gm6210023, JP21bm0704045, and JP21gm5010002h0004; and by the Takeda Science Foundation.

1. A. J. Cruz-Jentoft, A. A. Sayer, Sarcopenia. *Lancet* **393**, 2636–2646 (2019).
2. R. Furrer, C. Handschin, Muscle wasting diseases: Novel targets and treatments. *Annu. Rev. Pharmacol. Toxicol.* **59**, 315–339 (2019).
3. J. Fielitz *et al*., Myosin accumulation and striated muscle myopathy result from the loss of muscle RING finger 1 and 3. *J. Clin. Invest.* **117**, 2486–2495 (2007).
4. S. C. Bodine *et al*., Akt/mTOR pathway is a crucial regulator of skeletal muscle hypertrophy and can prevent muscle atrophy in vivo. *Nat. Cell Biol.* **3**, 1014–1019 (2001).
5. S. C. Bodine *et al*., Identification of ubiquitin ligases required for skeletal muscle atrophy. *Science* **294**, 1704–1708 (2001).
6. M. Sandri *et al*., Foxo transcription factors induce the atrophy-related ubiquitin ligase atrogin-1 and cause skeletal muscle atrophy. *Cell* **117**, 399–412 (2004).
7. M. D. Gomes, S. H. Lecker, R. T. Jagoe, A. Navon, A. L. Goldberg, Atrogin-1, a muscle-specific F-box protein highly expressed during muscle atrophy. *Proc. Natl. Acad. Sci. U.S.A.* **98**, 14440–14445 (2001).
8. D. S. Waddell *et al*., The glucocorticoid receptor and FOXO1 synergistically activate the skeletal muscle atrophy-associated MuRF1 gene. *Am. J. Physiol. Endocrinol. Metab.* **295**, E785–E797 (2008).
9. C. L. Wu, E. W. Cornwell, R. W. Jackman, S. C. Kandarian, NF-κB but not FoxO sites in the MuRF1 promoter are required for transcriptional activation in disuse muscle atrophy. *Am. J. Physiol. Cell Physiol.* **306**, C762–C767 (2014).
10. C. Ninfali, L. Siles, D. S. Darling, A. Postigo, Regulation of muscle atrophy-related genes by the opposing transcriptional activities of ZEB1/CtBP and FOXO3. *Nucleic Acids Res.* **46**, 10697–10708 (2018).
11. B. B. McConnell, V. W. Yang, Mammalian Krüppel-like factors in health and diseases. *Physiol. Rev.* **90**, 1337–1381 (2010).
12. N. M. Pollak, M. Hoffman, I. J. Goldberg, K. Drosatos, Krüppel-like factors: Crippling and un-crippling metabolic pathways. *JACC Basic Transl. Sci.* **3**, 132–156 (2018).
13. Y. Oishi, I. Manabe, Krüppel-like factors in metabolic homeostasis and cardiometabolic disease. *Front. Cardiovasc. Med.* **5**, 69 (2018).
14. D. A. Prosdocimo, M. K. Sabeh, M. K. Jain, Kruppel-like factors in muscle health and disease. *Trends Cardiovasc. Med.* **25**, 278–287 (2015).
15. Y. Oishi *et al*., SUMOylation of Krüppel-like transcription factor 5 acts as a molecular switch in transcriptional programs of lipid metabolism involving PPAR-delta. *Nat. Med.* **14**, 656–666 (2008).
16. S. Hayashi, I. Manabe, Y. Suzuki, F. Relaix, Y. Oishi, Klf5 regulates muscle differentiation by directly targeting muscle-specific genes in cooperation with MyoD in mice. *eLife* **5**, e17462 (2016).
17. T. Shindo *et al*., Krüppel-like zinc-finger transcription factor KLF5/BTEB2 is a target for angiotensin II signaling and an essential regulator of cardiovascular remodeling. *Nat. Med.* **8**, 856–863 (2002).
18. K. Fujiu *et al*., Synthetic retinoid Am80 suppresses smooth muscle phenotypic modulation and in-stent neointima formation by inhibiting KLF5. *Circ. Res.* **97**, 1132–1141 (2005).
19. X. H. Zhang, B. Zheng, M. Han, S. B. Miao, J. K. Wen, Synthetic retinoid Am80 inhibits interaction of KLF5 with RAR alpha through inducing KLF5 dephosphorylation mediated by the PI3K/Akt signaling in vascular smooth muscle cells. *FEBS Lett.* **583**, 1231–1236 (2009).
20. M. Menconi *et al*., Role of glucocorticoids in the molecular regulation of muscle wasting. *Crit. Care Med.* **35**(9, suppl.)S602–S608 (2007).
21. O. Schakman, S. Kalista, C. Barbé, A. Loumaye, J. P. Thissen, Glucocorticoid-induced skeletal muscle atrophy. *Int. J. Biochem. Cell Biol.* **45**, 2163–2172 (2013).
22. T. N. Stitt *et al*., The IGF-1/PI3K/Akt pathway prevents expression of muscle atrophy-induced ubiquitin ligases by inhibiting FOXO transcription factors. *Mol. Cell* **14**, 395–403 (2004).
23. B. A. Clarke *et al*., The E3 Ligase MuRF1 degrades myosin heavy chain protein in dexamethasone-treated skeletal muscle. *Cell Metab.* **6**, 376–385 (2007).
24. S. Cohen *et al*., During muscle atrophy, thick, but not thin, filament components are degraded by MuRF1-dependent ubiquitylation. *J. Cell Biol.* **185**, 1083–1095 (2009).
25. J. C. Brüning *et al*., A muscle-specific insulin receptor knockout exhibits features of the metabolic syndrome of NIDDM without altering glucose tolerance. *Mol. Cell* **2**, 559–569 (1998).
26. M. Yakabe *et al*., Inhibition of interleukin-6 decreases atrogene expression and ameliorates tail suspension-induced skeletal muscle atrophy. *PLoS One* **13**, e0191318 (2018).
27. S. W. Tobin *et al*., Regulation of Hspb7 by MEF2 and AP-1: Implications for Hspb7 in muscle atrophy. *J. Cell Sci.* **129**, 4076–4090 (2016).
28. J. Nordquist *et al*., Transcription factors in muscle atrophy caused by blocked neuromuscular transmission and muscle unloading in rats. *Mol. Med.* **13**, 461–470 (2007).
29. B. T. O'Neill *et al*., FoxO transcription factors are critical regulators of diabetes-related muscle atrophy. *Diabetes* **68**, 556–570 (2019).
30. M. P. Creyghton *et al*., Histone H3K27ac separates active from poised enhancers and predicts developmental state. *Proc. Natl. Acad. Sci. U.S.A.* **107**, 21931–21936 (2010).
31. S. R. Jesinkey, M. C. Korrapati, K. A. Rasbach, C. C. Beeson, R. G. Schnellmann, Atomoxetine prevents dexamethasone-induced skeletal muscle atrophy in mice. *J. Pharmacol. Exp. Ther.* **351**, 663–673 (2014).
32. Mahmassani ZS *et al*., Age-dependent skeletal muscle transcriptome response to bed rest-induced atrophy. *J. Appl. Physiol. (1985)* **126**, 894–902 (2019).
33. C. Ubaida-Mohien *et al*., Discovery proteomics in aging human skeletal muscle finds change in spliceosome, immunity, proteostasis and mitochondria. *eLife* **8**, e49874 (2019).
34. E. Migliavacca *et al*., Mitochondrial oxidative capacity and NAD^+ biosynthesis are reduced in human sarcopenia across ethnicities. *Nat. Commun.* **10**, 5808 (2019).
35. G. H. Zhu *et al*., Activation of RXR and RAR signaling promotes myogenic differentiation of myoblastic C2C12 cells. *Differentiation* **78**, 195–204 (2009).
36. M. El Haddad *et al*., Retinoic acid maintains human skeletal muscle progenitor cells in an immature state. *Cell. Mol. Life Sci.* **74**, 1923–1936 (2017).
37. C. Krueger, F. M. Hoffmann, Identification of retinoic acid in a high content screen for agents that overcome the anti-myogenic effect of TGF-beta-1. *PLoS One* **5**, e15511 (2010).
38. J. Amengual *et al*., Retinoic acid increases fatty acid oxidation and irisin expression in skeletal muscle cells and impacts irisin in vivo. *Cell. Physiol. Biochem.* **46**, 187–202 (2018).
39. A. Ruiz *et al*., Over-expression of a retinol dehydrogenase (SRP35/DHRS7C) in skeletal muscle activates mTORC2, enhances glucose metabolism and muscle performance. *Sci. Rep.* **8**, 636 (2018).
40. A. Di Rocco *et al*., Selective retinoic acid receptor γ agonists promote repair of injured skeletal muscle in mouse. *Am. J. Pathol.* **185**, 2495–2504 (2015).
41. L. Zhao *et al*., Retinoic acid signalling in fibro/adipogenic progenitors robustly enhances muscle regeneration. *EBioMedicine* **60**, 103020 (2020).
42. W. C. Chen, H. H. Lin, M. J. Tang, Matrix-stiffness-regulated inverse expression of Krüppel-like factor 5 and Krüppel-like factor 4 in the pathogenesis of renal fibrosis. *Am. J. Pathol.* **185**, 2468–2481 (2015).
43. X. R. Lv *et al*., Synthetic retinoid Am80 up-regulates apelin expression by promoting interaction of RARα with KLF5 and Sp1 in vascular smooth muscle cells. *Biochem. J.* **456**, 35–46 (2013).
44. P. Sousa-Victor *et al*., Geriatric muscle stem cells switch reversible quiescence into senescence. *Nature* **506**, 316–321 (2014).
45. B. D. Cosgrove *et al*., Rejuvenation of the muscle stem cell population restores strength to injured aged muscles. *Nat. Med.* **20**, 255–264 (2014).
46. S. Tümpel, K. L. Rudolph, Quiescence: Good and bad of stem cell aging. *Trends Cell Biol.* **29**, 672–685 (2019).
47. D. Walter *et al*., Exit from dormancy provokes DNA-damage-induced attrition in haematopoietic stem cells. *Nature* **520**, 549–552 (2015).
48. L. M. Oliveira, F. M. E. Teixeira, M. N. Sato, Impact of retinoic acid on immune cells and inflammatory diseases. *Mediators Inflamm.* **2018**, 3067126 (2018).
49. W. Balkan, M. Rodríguez-Gonzalez, M. Pang, I. Fernandez, B. R. Troen, Retinoic acid inhibits NFATc1 expression and osteoclast differentiation. *J. Bone Miner. Metab.* **29**, 652–661 (2011).
50. Y. Hirata *et al*., Hyperglycemia induces skeletal muscle atrophy via a WWP1/KLF15 axis. *JCI Insight* **4**, 124952 (2019).
51. N. Shimizu *et al*., Crosstalk between glucocorticoid receptor and nutritional sensor mTOR in skeletal muscle. *Cell Metab.* **13**, 170–182 (2011).
52. A. Morrison-Nozik *et al*., Glucocorticoids enhance muscle endurance and ameliorate Duchenne muscular dystrophy through a defined metabolic program. *Proc. Natl. Acad. Sci. U.S.A.* **112**, E6780–E6789 (2015).
53. S. Gray *et al*., Regulation of gluconeogenesis by Krüppel-like factor 15. *Cell Metab.* **5**, 305–312 (2007).
54. L. Fan, P. N. Hsieh, D. R. Sweet, M. K. Jain, Krüppel-like factor 15: Regulator of BCAA metabolism and circadian protein rhythmicity. *Pharmacol. Res.* **130**, 123–126 (2018).
55. S. H. Kang *et al*., Forkhead box O3 plays a role in skeletal muscle atrophy through expression of E3 ubiquitin ligases MuRF-1 and atrogin-1 in Cushing's syndrome. *Am. J. Physiol. Endocrinol. Metab.* **312**, E495–E507 (2017).
56. T. Hosaka *et al*., Disruption of forkhead transcription factor (FOXO) family members in mice reveals their functional diversification. *Proc. Natl. Acad. Sci. U.S.A.* **101**, 2975–2980 (2004).
57. F. B. Berry *et al*., FOXC1 is required for cell viability and resistance to oxidative stress in the eye through the transcriptional regulation of FOXO1A. *Hum. Mol. Genet.* **17**, 490–505 (2008).
58. B. E. Phillips *et al*., Molecular networks of human muscle adaptation to exercise and age. *PLoS Genet.* **9**, e1003389 (2013).
59. Y. Hashimoto, H. Kagechika, E. Kawachi, K. Shudo, Specific uptake of retinoids into human promyelocytic leukemia cells HL-60 by retinoid-specific binding protein: Possibly the true retinoid receptor. *Jpn. J. Cancer Res.* **79**, 473–483 (1988).
60. H. Kagechika, E. Kawachi, Y. Hashimoto, T. Himi, K. Shudo, Retinobenzoic acids. 1. Structure-activity relationships of aromatic amides with retinoidal activity. *J. Med. Chem.* **31**, 2182–2192 (1988).
61. K. Hirasaka *et al*., Clinorotation prevents differentiation of rat myoblastic L6 cells in association with reduced NF-kappa B signaling. *Biochim. Biophys. Acta* **1743**, 130–140 (2005).
62. A. Dobin *et al*., STAR: Ultrafast universal RNA-seq aligner. *Bioinformatics* **29**, 15–21 (2013).

MEDICAL SCIENCES

63. S. Heinz *et al*., Simple combinations of lineage-determining transcription factors prime cis-regulatory elements required for macrophage and B cell identities. *Mol. Cell* **38**, 576–589 (2010).
64. M. I. Love, W. Huber, S. Anders, Moderated estimation of fold change and dispersion for RNA-seq data with DESeq2. *Genome Biol.* **15**, 550 (2014).
65. Y. Zhou *et al*., Metascape provides a biologist-oriented resource for the analysis of systems-level datasets. *Nat. Commun.* **10**, 1523 (2019).
66. J. D. Buenrostro, P. G. Giresi, L. C. Zaba, H. Y. Chang, W. J. Greenleaf, Transposition of native chromatin for fast and sensitive epigenomic profiling of open chromatin, DNA-binding proteins and nucleosome position. *Nat. Methods* **10**, 1213–1218 (2013).
67. ENCODE Project Consortium, An integrated encyclopedia of DNA elements in the human genome. *Nature* **489**, 57–74 (2012).
68. C. Y. McLean *et al*., GREAT improves functional interpretation of cis-regulatory regions. *Nat. Biotechnol.* **28**, 495–501 (2010).
69. J. M. Jones *et al*., An assessment of myotube morphology, matrix deformation, and myogenic mRNA expression in custom-built and commercially available engineered muscle chamber configurations. *Front. Physiol.* **9**, 483 (2018).
70. C. Rommel *et al*., Mediation of IGF-1-induced skeletal myotube hypertrophy by PI(3)K/Akt/mTOR and PI(3)K/Akt/GSK3 pathways. *Nat. Cell Biol.* **3**, 1009–1013 (2001).
71. C. C. Agley, C. P. Velloso, N. R. Lazarus, S. D. Harridge, An image analysis method for the precise selection and quantitation of fluorescently labeled cellular constituents: Application to the measurement of human muscle cells in culture. *J. Histochem. Cytochem.* **60**, 428–438 (2012).
72. A. Bettadapur *et al*., Prolonged culture of aligned skeletal myotubes on micromolded gelatin hydrogels. *Sci. Rep.* **6**, 28855 (2016).
73. A. J. Saldanha, Java Treeview—Extensible visualization of microarray data. *Bioinformatics* **20**, 3246–3248 (2004).